

N. Sepasian
Department of Biomedical Engineering
TU Eindhoven
5600 MB Eindhoven
n.sepasian@tue.nl

J.H.M. ten Thije Boonkamp
Department of Mathematics and Computer
Science
TU Eindhoven
5600 MB Eindhoven
j.h.m.tenthijeboonkamp@tue.nl

A. Vilanova
Department of Electrical Engineering, Math-
ematics and Computer Science
TU Delft
2628 CD Delft
A.Vilanova@tudelft.nl

Diffusion Tensor Imaging: Brain Pathway Reconstruction

Diffusion tensor imaging (DTI) is a recently developed modality of magnetic resonance imaging (MRI), which allows producing in-vivo images of biological fibrous tissues such as the neural axons of white matter in the brain. The techniques for reconstructing connections between different brain areas using DTI are collectively known as fiber tracking or tractography. The brain connectivity map, derived from the tractography visualization and analysis, is an important tool to diagnose and analyze various brain diseases, and is of essential value in providing exquisite details on tissue microstructure and neural networks.

Assuming that fiber pathways follow the most efficient diffusion propagation trajectories, we specifically develop a geodesic-based tractography technique for the reconstruction of fiber pathways. Results we obtain using our technique, based on finding multiple geodesics connecting two given points or regions are encouraging and give confidence that this method can be used for practical purposes in the near future.

1. Brain Structure

The nervous system functions as the body's communication and decision center. The brain and spinal cord are collectively known as central nervous system. Brain and spinal cord are made of grey matter and white matter. White matter consist mostly of myelinated axons and non-neural cells. Grey matter is a type of neural tissue mainly consisting of dendrites and both unmyelinated and myelinated axons. The grey matter takes care of the processing functions whereas the white matter provides the communication between different grey matter areas and the rest of the body. Sensory nerves gather the information from

the environment and send them to the spinal cord. The spinal cord sends this information to the brain.

The white matter axons are surrounded by myelin; see Figure 1¹. The myelin gives the whitish appearance to the white matter. Myelin increases the speed of transmission of all nerve signals and is distributed diffusely or is concentrated in bundles. These bundles are often referred to as tracts or fiber pathways. Our goal is to develop accurate mathematical models for in-vivo reconstruction of brain fiber bundles to study a host of various disorders and neurodegenerative diseases including, among others, Parkinson, Alzheimer and Huntington.

2. Diffusion Process

It is known that a significant amount of the human body consists of water. At a microscopic scale water molecules move freely and collide with each other. This movement of water molecules is known as Brownian motion, which implies that molecules in a uniform volume of water will diffuse randomly in all directions. At a macroscopic scale, this phenomenon is known as diffusion. Diffusion is the thermal motion of all (liquid and gas) molecules at temperatures above absolute zero. Depending on the medium, diffusion can be either *isotropic* or *anisotropic*. Figure 2 illustrates the difference between diffusion processes in different media. For free or isotropic diffusion, the probability distribution of a single molecule located at position \mathbf{x}_0 to reach another position \mathbf{x}_1 after a given time t is spherically symmetric, i.e., every direction is equally probable. This is illustrated in Figure 2(a).

Einstein [2] describes diffusion by relating the diffusion coefficient D , which characterizes the mobility of the molecules, to the root mean square of the diffusion displacement, i.e.,

$$(1) \quad D = \frac{1}{6t} \langle \mathbf{R}^T \mathbf{R} \rangle.$$

¹<http://www.adameducation.com/>

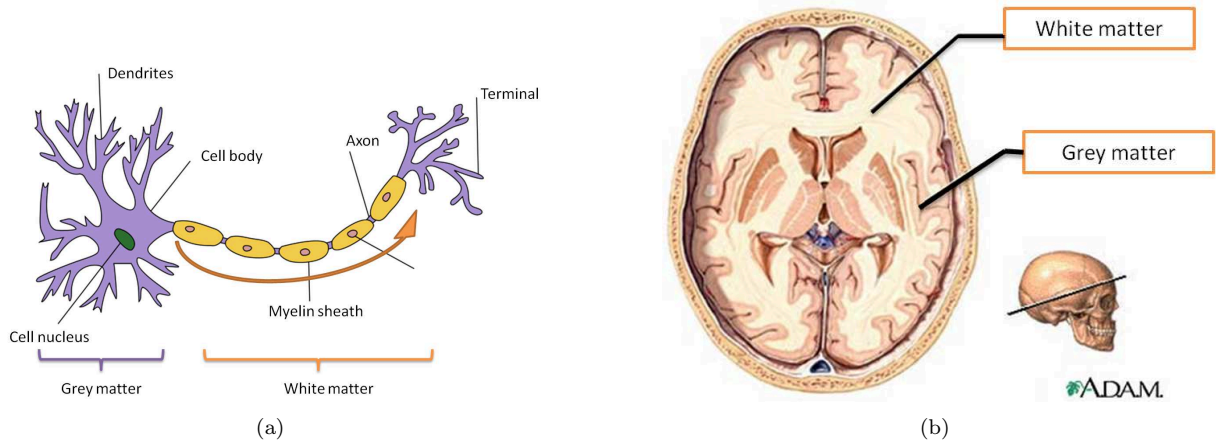


FIGURE 1. (a) Structure of a typical core component (neuron) of the central nervous system, (b) Axial view of a brain illustrating white and grey matter.

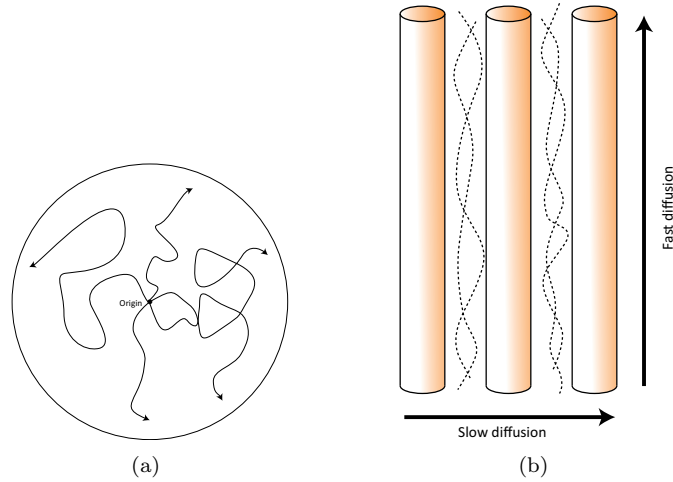


FIGURE 2. (a) Isotropic diffusion, (b) Anisotropic diffusion. The arrows indicate possible trajectories which molecules may follow. In the presence of barriers, e.g. axons, diffusion is restricted in certain directions.

In this expression \mathbf{R} is the net displacement vector $\mathbf{R} = \mathbf{x}_1 - \mathbf{x}_0$. The bracket $\langle \rangle$ denotes the ensemble average. In the isotropic case, the scalar D depends on the molecule type and the medium properties but not on the direction.

Using Fick's law of diffusion, the diffusion process can be approximated as follows [3]:

$$(2) \quad \frac{\partial P(\mathbf{R}, t)}{\partial t} = D \nabla^2 P(\mathbf{R}, t).$$

Here, ∇^2 is the Laplacian in \mathbf{R} and $P(\mathbf{R}, t)$ represents the probability of a water molecule displacement \mathbf{R} in time t , and is known as the diffusion displacement probability density function (PDF). Under the condition

$$(3) \quad \int_{\mathbf{R}^3} P(\mathbf{R}, t) d\mathbf{R} = 1,$$

the solution to equation (2) is a Gaussian distribution and can be written as

$$(4) \quad P(\mathbf{R}, t) = \frac{1}{\sqrt{(4\pi Dt)^3}} \exp\left(\frac{-1}{4Dt} \mathbf{R}^T \mathbf{R}\right).$$

In anisotropic biological tissues, the mobility of water molecules is restricted by obstacles formed by surrounding structures, such as the axons in the brain; see Figure 2(b). It is known that myelin sheaths have a property to modulate the anisotropy of diffusion [5].

Several models have been proposed for the PDF of anisotropic diffusion. Amongst these models, the most popular one is known as the diffusion tensor (DT) model [6]. In this model of water diffusion, Einstein's law of diffusion is generalized to anisotropic diffusion by replacing the scalar diffusion coefficient D in (1) by a symmetric

positive definite matrix \mathbf{D} , as follows

$$(5) \quad \mathbf{D} = \begin{pmatrix} d_{11} & d_{12} & d_{13} \\ d_{12} & d_{22} & d_{23} \\ d_{13} & d_{23} & d_{33} \end{pmatrix} = \frac{1}{6t} \langle \mathbf{R}\mathbf{R}^T \rangle.$$

Analogously, equation (2) generalizes to

$$(6) \quad \frac{\partial P(\mathbf{R}, t)}{\partial t} = \nabla \cdot (\mathbf{D} \nabla P(\mathbf{R}, t)).$$

The solution of (6) is a Gaussian distribution and gives the diffusion PDF of water molecules. Given the condition (3), it can be written as

$$(7) \quad P(\mathbf{R}, t) = \frac{1}{\sqrt{(4\pi t)^3 |\mathbf{D}|}} \exp\left(\frac{-1}{4t} \mathbf{R}^T \mathbf{D}^{-1} \mathbf{R}\right),$$

where $|\mathbf{D}| > 0$ is the determinant of \mathbf{D} .

3. Acquisition and Reconstruction of Diffusion

Diffusion-weighted magnetic resonance imaging (DWMRI) is an acquisition technique to measure the random Brownian motion of water molecules within a voxel of tissue. This technique provides a unique non-invasive tool for measuring the local characteristics of tissues. The first diffusion weighted imaging (DWI) acquisition was done by Taylor *et al.* [4] using a hens egg as a phantom in a small bore magnet. Later, Le Bihan *et al.* [7] applied the first DWI acquisition for the human brain on a whole body scan.

To obtain diffusion weighted images, a pair of strong gradient pulses of a magnetic field, which defines the direction in which the diffusion is measured, is applied. The diffusion weighting sequence is commonly known as the so-called Stejskal-Tanner sequence. Since the diffusion probability distribution function has assumed to be Gaussian, the attenuated signal of the Stejskal-Tanner sequence in relation to \mathbf{D} is specified as follows,

$$(8) \quad S(\mathbf{y}) = S_0 e^{-b\mathbf{y}^T \mathbf{D} \mathbf{y}},$$

where \mathbf{y} is a unit vector in the diffusion gradient direction and $S(\mathbf{y})$ is the associated signal. Here b represents the so-called b -value and is the diffusion weighting factor depending on scanner parameters and S_0 is the reference nuclear magnetic resonance signal.

Given multiple diffusion weighted images, we can measure quantitative scalars such as the apparent diffusion coefficient (ADC), which describe the diffusion process. The ADC is given by the relation

$$(9) \quad D(\mathbf{y}) = -\frac{1}{b} \ln\left(\frac{S(\mathbf{y})}{S_0}\right).$$

The ADC in anisotropic tissues varies depending on the direction \mathbf{y} in which it is measured; see Figure 3. To model the intrinsic diffusion properties of biological tissues, Basser *et al.* proposed to fit the DWI data to a second order symmetric and positive-definite tensor \mathbf{D} [9].

To this end, one can write the relation between the ADC and the diffusion tensor \mathbf{D} as follows,

$$(10) \quad D(\mathbf{y}_i) = \mathbf{y}_i^T \mathbf{D} \mathbf{y}_i = \sum_{\beta=1}^3 \sum_{\alpha=1}^3 d_{\alpha\beta} \mathbf{y}_i^\alpha \mathbf{y}_i^\beta,$$

for $i = 1, 2, \dots, n$ with n the number of sampled gradient directions. Using relation (10), the six unknown coefficients of the diffusion tensor \mathbf{D} can be computed by choosing at least six gradient directions, typically we take $20 \leq n \leq 60$. Relation (10) gives rise to an over-determined system and can be solved using least squares fitting [17]. This is in fact the same diffusion tensor (DT) as introduced earlier in Einstein's equation (5) for anisotropic diffusion.

The DT is determined by its three eigenvalues $\lambda_1 \geq \lambda_2 \geq \lambda_3 > 0$ and its three corresponding orthogonal eigenvectors $\mathbf{e}_1, \mathbf{e}_2, \mathbf{e}_3$. The largest eigenvalue λ_1 gives the principal direction \mathbf{e}_1 of the diffusion tensor. Note that the other two eigenvectors span the plane orthogonal to the main eigenvector. Using the three eigenvalues and their corresponding eigenvectors a DT can be visualized as an ellipsoid which corresponds to the implicit surface $\{\mathbf{R} : \mathbf{R}^T \mathbf{D}^{-2} \mathbf{R} = \text{const}\}$ [19, 18]. Figure 4(b)-4(a) are illustrations of these procedures. Figure 4(c) shows the diffusion tensor field for a slice of a brain image.

Diffusion tensor images are useful when the tissue of interest is dominated by isotropic water movement such as grey matter in the cerebral cortex, where the diffusion time appears to be the same along any axis. Therefore, they are for example applicable to diagnose vascular strokes in the brain. However, in the cases where the direction and shape of the diffusion propagation is important, the resulting image using this technique is difficult to interpret directly and does not provide much information about the underlying fibrous structure. This is particularly crucial for analysing the white matter structure. Therefore, further reconstruction techniques have been developed in order to extract more useful information from these images.

4. Reconstruction of Brain Fiber Tracts

Due to the fibrous structure of white matter, diffusion of water molecules is dominant in the direction of the fibers. As we described before, diffusion and its directional variation can be measured by DWI. The process of reconstructing fibers using DWI is commonly known as tractography or fiber tracking.

In clinics, the most commonly used DTI tractography algorithms are principal diffusion direction (PDD) methods [3] where the fibers are integrated along the main eigenvector field $\mathbf{e}_1(\mathbf{x})$ of the diffusion tensor. This is numerically equivalent to solving the initial value problem

$$(11) \quad \begin{cases} \dot{\mathbf{x}} = \mathbf{e}_1(\mathbf{x}(t)), & t > 0, \\ \mathbf{x}(0) = \mathbf{x}_0. \end{cases}$$

Here \mathbf{x}_0 denotes the initial position or seed point and t is the time. The initial value problem (11) can be solved

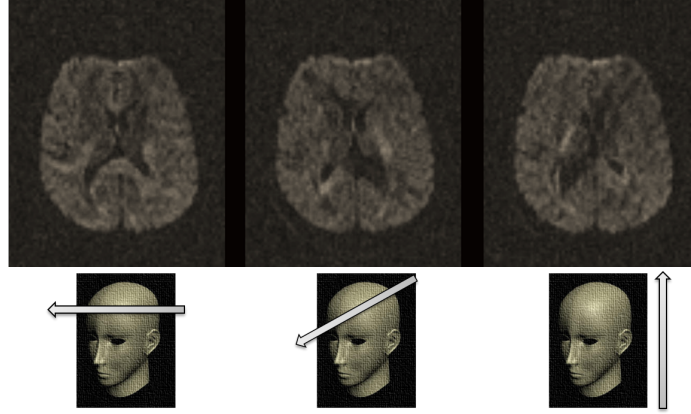


FIGURE 3. Diffusion-weighted images with three different acquisition directions. Note the differences in contrast as the gradient direction is changing. Arrows indicate the gradient directions. Adapted from Campbell [3].

using a fourth-order Runge-Kutta method. Figure 5 illustrates an example of PDD tractography.

The PDD methods just employ local information and are therefore sensitive to noise. Small changes can produce completely different results or undesired fiber pathways; see Figure 6. A relatively small amount of noise in the diffusion tensor field causes accumulative errors in the trajectory of the fibers. Tackling this problem in tractography algorithms has been a main inspiration for introducing many variations of PDD tractography. Moreover, it has been recently shown that the expected properties of actual fibers, such as fanning, cannot be reconstructed using PDD based tractography [15]. To overcome this problem, advanced models, such as global geometric tractography methods, were developed to deduce connectivity in the white matter by globally optimizing a certain cost function on the basis of the diffusion tensor information. The goal of global geometric tractography is to find optimal paths that connect two given regions/points. This can potentially overcome accumulative errors introduced in tractography due to local noise. Besides, these models use the whole diffusion tensor profile instead of reducing this information into a single direction of the main eigenvector.

5. Geodesics for Tractography

In order to reconstruct the globally optimal pathways we assume that fiber tracts coincide with geodesics in the Riemannian manifold defined using the inverse of the diffusion tensor as metric. The rationale behind this assumption is that water molecules move freely along fiber tracts, and their movement is restricted in the perpendicular directions. Therefore, it is assumed that the fiber connecting two points follows the most efficient diffusion path for water molecules. We are searching for a path that maximizes diffusion. This can be achieved by inverting the metric that converts the largest eigenvalue into the smallest one.

Therefore, we choose $\mathbf{G} = (g_{\alpha\beta}) = \mathbf{D}^{-1}$ with \mathbf{D} defined in (5). Consequently, the geodesics for this metric represent the fibers [10].

Thus, consider a bounded curve \mathcal{C} , with parametrization $\mathbf{x} = \boldsymbol{\chi}(\tau)$, $a \leq \tau \leq b$. A geodesic between two points $\boldsymbol{\chi}(a)$ and $\boldsymbol{\chi}(b)$ is the smooth curve whose length is the minimum of all possible lengths. In the following we use the Einstein notation, i.e., we sum over repeated indices, one in the upper (superscript) and one in the lower (subscript) position. For a general metric $ds^2 = g_{\alpha\beta} dx^\alpha dx^\beta$, the length of \mathcal{C} is given by

$$(12) \quad J[\boldsymbol{\chi}] = \int_{\mathcal{C}} ds = \int_a^b (g_{\alpha\beta}(\boldsymbol{\chi}(\tau)) \dot{\chi}^\alpha(\tau) \dot{\chi}^\beta(\tau))^{1/2} d\tau.$$

The metric tensor $(g_{\alpha\beta})$ only depends on \mathbf{x} , and is symmetric positive definite. The solution to the so-called geodesic equations minimizes $J[\boldsymbol{\chi}]$. These are given by

$$(13) \quad \ddot{x}^\alpha + \Gamma_{\beta\gamma}^\alpha \dot{x}^\beta \dot{x}^\gamma = 0,$$

where $\Gamma_{\beta\gamma}^\alpha$ is the Christoffel symbol of the second kind, defined by

$$(14) \quad \Gamma_{\beta\gamma}^\alpha = g^{\alpha\delta} [\beta\gamma, \delta],$$

where $[\beta\gamma, \alpha]$ is the Christoffel symbol of the first kind, and given by

$$(15) \quad [\beta\gamma, \alpha] = \frac{1}{2} \left(\frac{\partial g_{\alpha\beta}}{\partial x^\gamma} + \frac{\partial g_{\alpha\gamma}}{\partial x^\beta} - \frac{\partial g_{\beta\gamma}}{\partial x^\alpha} \right).$$

Alternatively, we consider the functional that minimizes the length of all curves joining the fixed point $\boldsymbol{\chi}(a)$ and the time variable end point $\boldsymbol{\chi}(t)$, i.e.,

$$(16) \quad T(\mathbf{x}, t) = \min_{\boldsymbol{\chi}} \int_a^t (g_{\alpha\beta}(\boldsymbol{\chi}(\tau)) \dot{\chi}^\alpha(\tau) \dot{\chi}^\beta(\tau))^{1/2} d\tau,$$

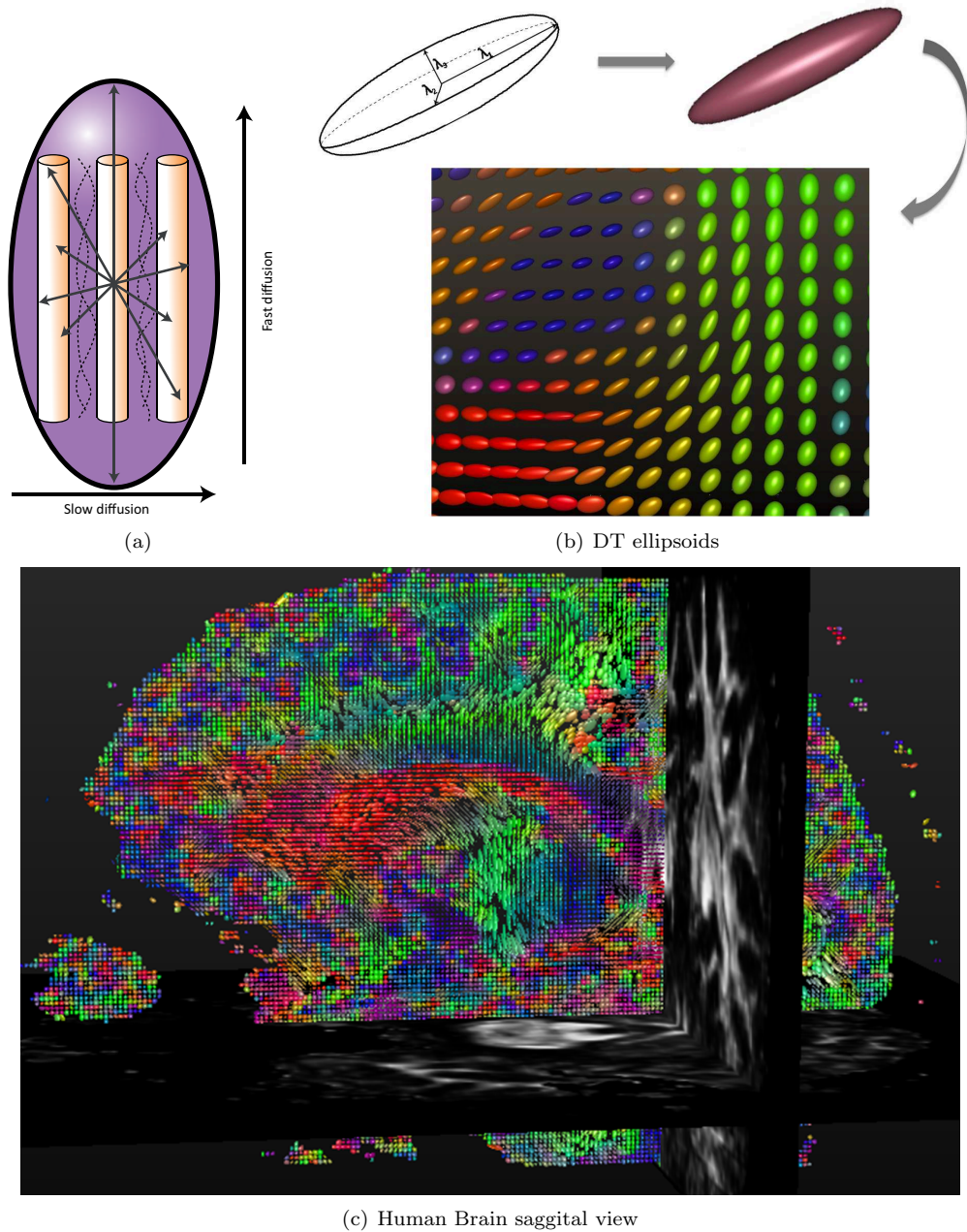


FIGURE 4. (a) Restricted diffusion process, (b) DT ellipsoids, (c) Saggital view of DT ellipsoids generated for a healthy Human Brain.

with $\mathbf{x} = \chi(t)$. The geodesic connecting $\chi(a)$ with $\chi(t)$ can be determined from the Hamilton-Jacobi (HJ) equation, given by

$$(17) \quad H\left(\mathbf{x}, \frac{\partial T}{\partial \mathbf{x}}\right) = 1,$$

where the Hamiltonian H is given by [11]

$$(18) \quad H^2(\mathbf{x}, \mathbf{p}) = g^{\alpha\beta}(\mathbf{x})p_\alpha p_\beta \quad p_\alpha := g_{\alpha\beta}(\mathbf{x})\dot{x}^\beta.$$

The HJ-equation may generate multi-valued solutions when, for example, there are discontinuities in the gradient field. Therefore, the viscosity solution is needed to ensure the existence and uniqueness of the solution to the HJ-equation [16]. This implies the viscosity solution is the minimum time; i.e. the first arrival time, for any curve from a given initial point to reach any other points inside the domain. Using the viscosity solution will not ensure that the solution we obtain is the real physically meaningful one; e.g., shortcuts when they are not desired. In order

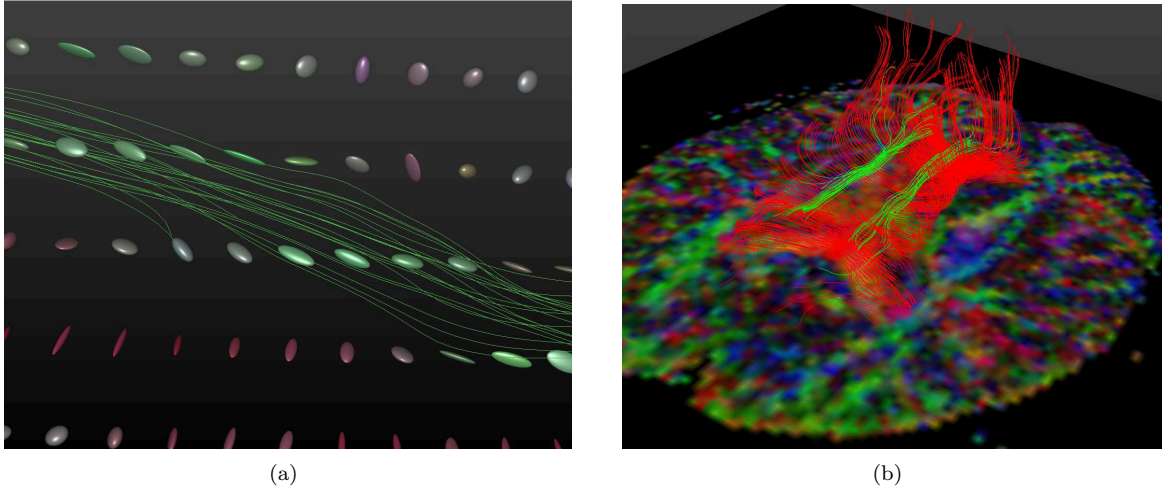


FIGURE 5. (a) Small group of fibers generated using PDD tractography. The main eigenvectors of the diffusion tensors determine the local orientation of the fibers. (b) Fibers generated by PDD tractography showing part of the cingulum and the corpus callosum.

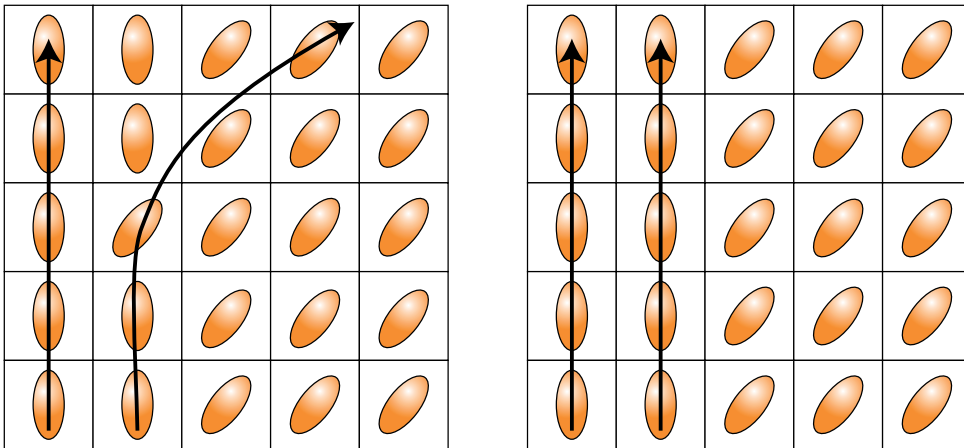


FIGURE 6. Illustration of the influence of noise in PDD tractography. Small changes in the direction of the tensor can cause deviation of the fiber from the actual pathway.

to tackle this issue, multi-valued solutions of the arrival time can be approximated by computing the geodesics directly from the geodesic equations [12, 8].

The geodesic equation (13) can be rewritten as the system of ordinary differential equations

$$(19) \quad \begin{aligned} \dot{x}^\alpha &= u^\alpha, \\ \dot{u}^\alpha &= -\Gamma_{\beta\gamma}^\alpha u^\beta u^\gamma. \end{aligned}$$

Consider $(x^1(0), x^2(0), x^3(0))$ as given initial point and $(u^1(0), u^2(0), u^3(0))$ as initial direction. We compute the solution of (19) for the given initial position and multiple initial directions using the standard fourth order explicit Runge-Kutta method. This gives us a set of geodesics for the given initial point and integrate till they hit the boundary of a given domain. Here, the domain is the outer surface of the brain.

6. Human Brain Fiber Reconstruction

We applied our proposed multi-valued geodesic tractography to reconstruct the fibrous tissue structure of the underlying neural axons of the white matter of a healthy human brain. Using available atlases of the human brain map [1], we select the region of interests. Geodesics are then computed until they meet one of the boundaries. To determine the fiber connecting two given regions we apply the line-plane intersection [12]. This allows us to cut off the geodesics once they enter one of the selected end regions.

Figure 7(a) shows the geodesics reconstructed for corticospinal tracts (top-right) and postcentral gyri areas of the corpus callosum using PDD (bottom-right) and multi-valued geodesics (bottom-left). Figure 7(b) illustrates the

results for the complete area of corpus callosum multi-valued geodesics.

Since there is no available ground truth for fiber bundles, simulated diffusion tensor data sets or white matter brain atlases are used for validating the tractography methods. We validate the results for our method with simulated phantoms and the report can be found in [8, 12]. Moreover, multi-valued geodesics tractography has been applied for various human brain data sets. According to clinical experts, multi-valued geodesics are more coherent with expected fiber tracts associated with the underlying bundles. Our model reconstructs the fanning tracts, particularly the ones connecting the cortex area, while those were completely missing using the PDD approach. Our proposed model has been integrated as a part of Vist/e biomedical visualization software and is publicly available ².

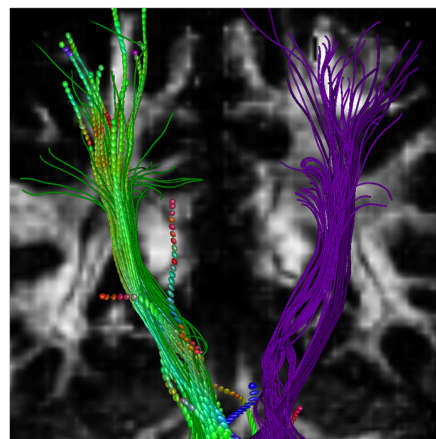
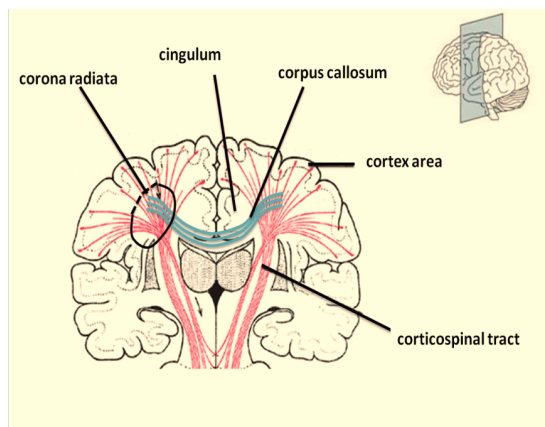
7. Future Work

Despite the simplicity of the DTI model, tractography techniques using the DT are shown to be very promising to reveal the structure of brain white matter. However, DTI assumes that each voxel contains fibers with only one single main orientation and it is known that brain white matter has multiple fiber orientations, which can be in many directions. High angular resolution diffusion imaging (HARDI) acquisition and its modeling techniques have been developed to overcome this limitation. The models applied to HARDI data result in a function on the sphere that gives information about the diffusion profile within the voxel [13]. An ongoing extension of geodesic based tractography models is to apply the previously discussed geodesic based models for the HARDI data [14]. Nevertheless, DTI is still widely used in clinical research due to either unavailability of the scanning protocols for HARDI or computationally expensive data processing. Therefore, improving existing methods and algorithms for DTI processing is beneficial for clinical purposes.

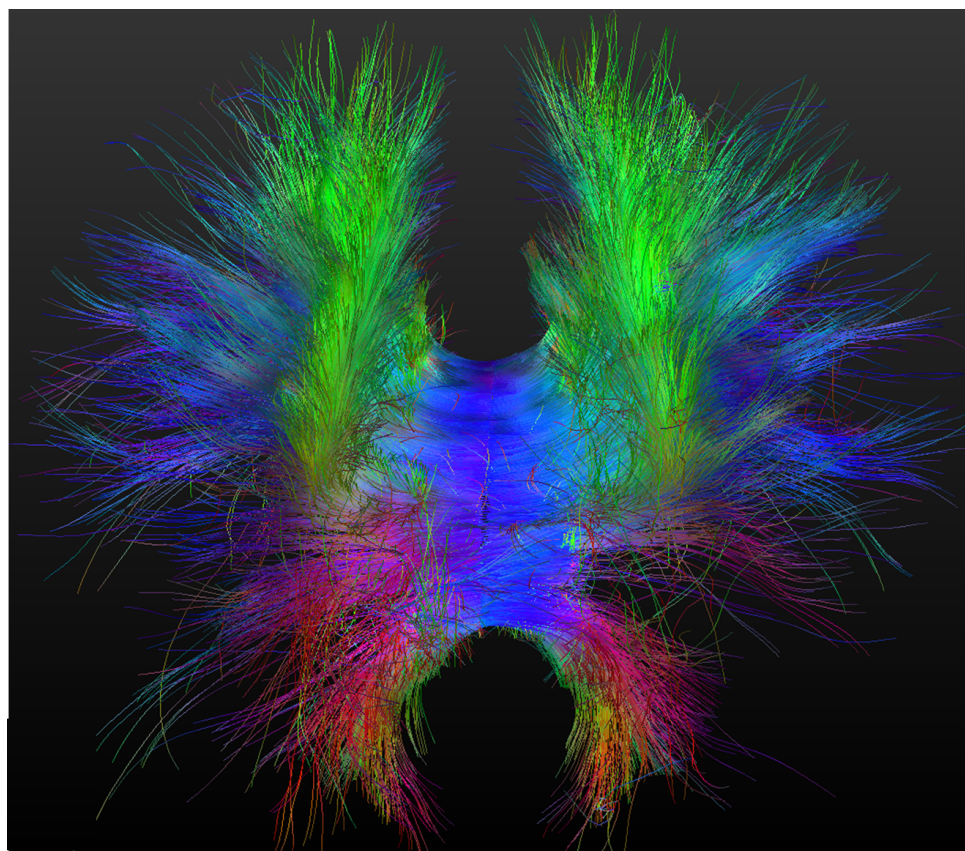
References

- [1] S. Mori *et al.* *MRI atlas of human white matter*, Elsevier, 2005.
- [2] A. Einstein, *Investigations on the theory of the Brownian movement*, Dover Publications, 1956.
- [3] J. S.W. Campbell, *Diffusion Imaging of White Matter Fibre Tracts*, Ph.D. Thesis, McGill University, 2004.
- [4] D. G. Taylor *et al.* *The spatial mapping of translational diffusion coefficients by the nmr imaging technique.*, Physics in Med. and Bio., McGill University, 30(4), 1985.
- [5] C. Beaulieu, *The basis of anisotropic water diffusion in the nervous system.* tech. rev. NMR in Biomed. 15:435–455, 2002.
- [6] P. Basser *et al.* *MR diffusion tensor spectroscopy and imaging.* Biophysical Journal, 66(1):259-267, 1994.
- [7] D. LeBihan *et al.* *Imagerie de diffusion in-vivo par résonance magnétique nucléaire.* Physics in Med. and Bio. 30(4), 1985.
- [8] N. Sepasian, *Multi-valued geodesic tractography for diffusion weighted imaging.* PhD thesis, Technische Universiteit Eindhoven, 2011.
- [9] P. J. Basser *et al.* *Spectral decomposition of a 4th-order covariance tensor: Applications to diffusion tensor MRI.* Signal Processing, 87:220–236, 2007.
- [10] V. Wedeen *et al.* *Mapping fiber orientation spectra in cerebral white matter with Fourier transform diffusion MRI.* Proceedings of the Intern. Soc. of Mag. Res. in Med. 2000.
- [11] H. Rund, *The Hamilton-Jacobi theory in the calculus of variations: its role in mathematics and physics*, Van Nostrand, 1966.
- [12] N. Sepasian *et al.* *Multivalued geodesic ray-tracing for computing brain connections using diffusion tensor imaging.* SIAM Journal on Imaging Sciences, 5(2), 483–504, 2012.
- [13] A. Fuster *et al.* *Riemann-Finsler geometry for diffusion weighted magnetic resonance imaging.* In Visualization and Processing of Tensors and Higher Order Descriptors for Multi-Valued Data (pp. 189-208). Springer, 2014.
- [14] N. Sepasian *et al.* *Riemann-Finsler multi-valued geodesic tractography for HARDI.* In Visualization and Processing of Tensors and Higher Order Descriptors for Multi-Valued Data, Mathematics and Visualization (pp. 209-225). Springer, 2014.
- [15] M. Bastiani *et al.* *Human cortical connectome reconstruction from diffusion weighted MRI: the effect of tractography algorithm.* Neuroimage. 62(3):1732-49, 2012.
- [16] C. Mantegazza *et al.* *Hamilton-Jacobi equations and distance functions on Riemannian manifolds.* App. Math. and Optim. 47(1):1-25, 2002.
- [17] P. J. Basser *et al.* *Estimation of the effective self-diffusion tensor from the NMR spin echo.* J Magn Reson B. 103(3):247-54, 1994.
- [18] T. Brox *et al.* *Nonlinear structure tensors.* 24(1), 41-55, Image and Vision Comput. 2006.
- [19] P. J. Basser *et al.* *Diffusion-tensor MRI: theory, experimental design and data analysis - a technical review.* NMR Biomed. 15(7-8):456-67, 2002.
- [20] H. Gray, *Anatomy of the Human Body.* The Bartleby edition, 1918.

²<https://sourceforge.net/projects/viste/>



(a)



(b)

FIGURE 7. Illustration of a healthy human brain fiber bundle reconstructions. (a) The motor tracts in red and corpus callosum tracts in blue modified from [20] (top-left), fibers reconstructed for corticospinal tracts using multi-valued geodesics (top-right) and postcentral gyri areas of the corpus callosum using PDD (bottom-right) and multi-valued geodesics (bottom-left). (b) Results for the complete area of corpus callosum multi-valued geodesics